Electronic Supplementary Materials

Tuning Non-doped Carbon Nanotubes to an Efficient Metal-free Electrocatalyst for Oxygen Reduction Reaction by Localizing the Orbital of Nanotubes with Topological Defects

Shujuan Jiang,[a] Zhe Li, * [b] Huayu Wang,[c] Yun Wang, [a] Lina Meng, [a] and Shaoqing Song*[a]

[a] *Key Laboratory of Radioactive Geology and Exploration Technology Fundamental Science for National Defense, School of Chemistry, Biology and Materials Science, East China Institute of Technology, Nanchang, Jiangxi Province 330013, P. R. China.*

[b] *Key Laboratory of Catalysis and Materials Science of the State Ethnic Affairs Commission &Ministry of Education, South-Central University for Nationalities, Wuhan, Hubei Province, 430074, P. R. China.*

[c] *Jiangxi University of Traditional Chinese Medicine, Nanchang, Jiangxi Province 330013, P. R. China.*

S1 Enlarged HRTEM images of TCNT and CNT samples in Figure 1 in the manuscript.

The enlarged images of HRTEM were presented here to illustrate the effect of convex and concave structures on the interplanar spacing of TCNTs. The straight CNTs have a layer spacing of 0.34 nm (Figure S1d, CNTs-3), while the interplanar spacing of TCNTs varies at different points with convex (white marks) and concave (blue marks) structures. However, all the lattice space, regardless of the convex or concave structure, is smaller than 0.34 nm of the straight nanotubes, which may be caused by the oppression between layers during the formation of topological defects.

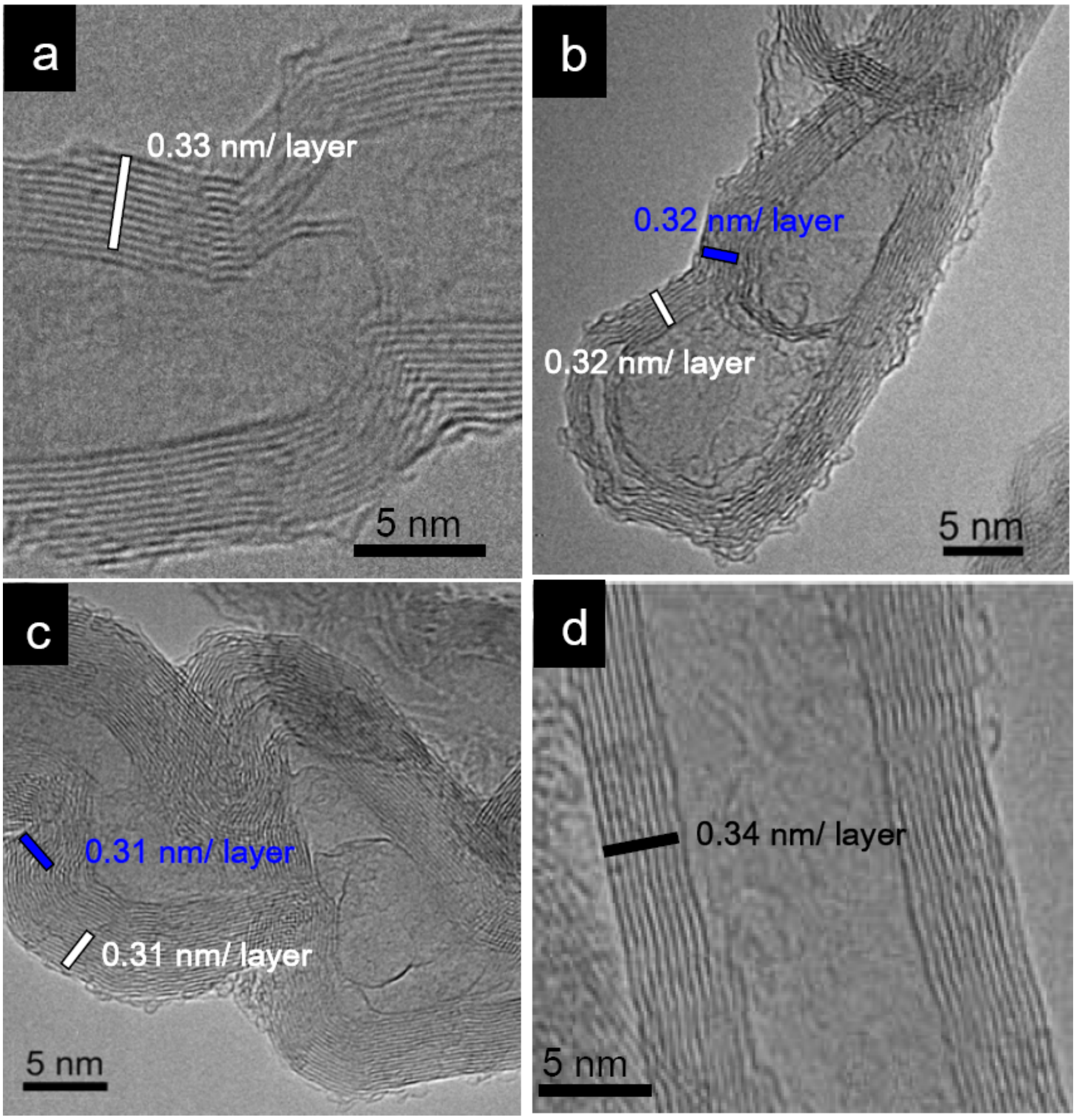

Figure S1. The enlarged images of HRTEM in Figure 1of the main text. (a) TCNTs-1, (b) TCNTs-2, (c) TCNTs-3 and (d) CNTs-3.

S2 XPS and XRD results for the CNTs and TCNTs

XPS was employed to analyze the samples. The full XPS survey spectra for the CNTs, TCNTs-1, TCNTs-2 and TCNTs-3 are shown in Figure S2. Each sample are composed of the predominant C and trace of O, and the oxygen content is similar to be 1.12, 1.04, 1.36 and 1.76 at% corresponding to TCNTs-3, TCNTs-2, TCNTs-1 and CNTs (Figure S2A). There is trace amount of O in each nanotube samples even with benzene as precursor, indicating that the O impurity in all the samples was introduced during the post-purification treatment but not from the O doping. Therefore, the only possible heteroatom oxygen doping can be excluded and the morphology evolution for TCNT samples is definitely caused by the induction of topological defects. The topological defect density in TCNTs cannot be differed by C 1s XPS as reflected by the similar C chemical component distribution of sp^2 and sp^3 in CNTs and TCNTs due to the limitation of XPS technique (Figure S2B).

The further information from the fine spectra analysis show that the contents of Co 2p, and Al 2p are all below the detection limit but there are trace amount of Fe (0.2 at%) (Figure S2C). However, the effect of the residue Fe atoms can be negligible because there are only two atoms in per 1000 atoms in TCNTs, which indicates an effective and mild purification method of NaOH/HCl treatment. Furthermore, the XRD patterns in Figure S2D show that the three peaks for TCNTs at 26.1°, 43.8° and 54.2° are attributed to the (002), (100) and (004) diffractions of graphite in the CNTs and TCNTs (JCPDS 41-1487), and there is no other signals for Fe, Co or Al components. Therefore, the XRD and XPS results have deducted the obscurity of the possible heteroatom doping and metal residue in TCNTs.

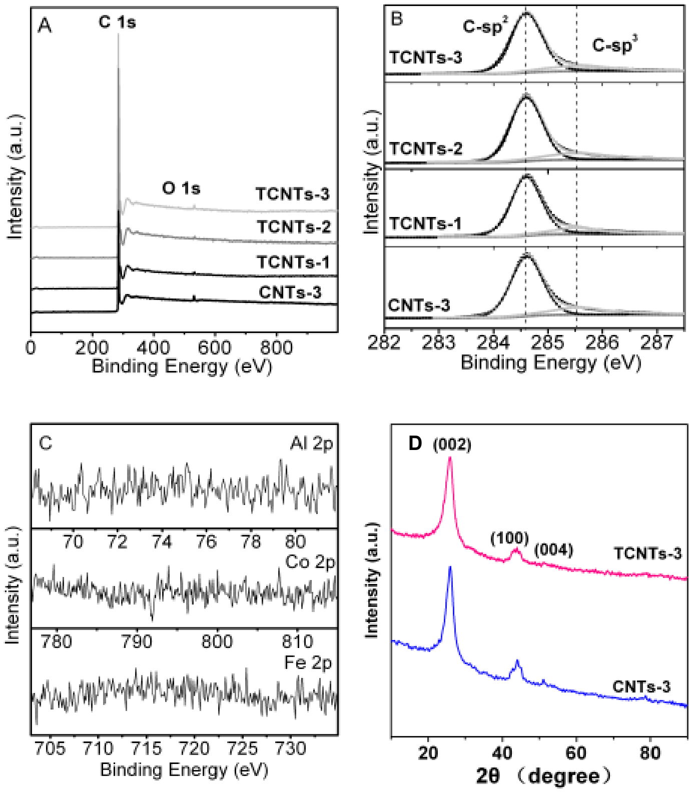

Figure S2. Survey (A) and fine XPS spectra (B, C) as well as XRD (D) results for CNTs and TCNTs. The peaks in XPS are calibrated by the center peak of C 284.6 eV.

S3 The side and top views of the PCNT(5,5) models

The side and top views of the PCNT(5,5) models with single, double and triple pentagon(s) are given and the pentagon structure is highlighted by cyan color, as shown in Figure S5. It is obvious that the introduction of pentagon structure brings a positive curvature to CNT, and with increasing the pentagon number from single, double to triple, the curvature of PCNT increases gradually. The introduction of heptagon in CNT(5,5) produces a negative curvature to CNT, and the curvature becomes apparent along with increasing the numbers of heptagon, which is not presented here.

a

b

c

Figure S5. The side view and top view of the PCNT(5,5) models with (a) single, (b) double and (c) triple pentagon(s). The pentagon structure is highlighted by cyan color.

S4 The influence of the graphene-like edges in TCNT catalysts on ORR

It is known that the graphene-like edge defect forms more or less on the side walls of carbon-based nanotubes unavoidably during the nanotube growth and the following purification treatment. To investigate the effect of these defects on the activity of TCNTs, the comparison experiment was performed. CNTs-D with great amount of graphene-like edges was obtained by via a ball milling approach to CNTs-1, confirmed by TEM (Figure S3a). After a 36 min ball milling treatment, the I_D/I_G in Raman spectrum of CNTs-D (Figure S3b) was 0.9 which is similar to that of the TCNTs-1 (Figure 2 in the main text). In the CV tests, CNTs with graphene-like edges showed slightly higher electrocatalytic activity than CNTs-1, but obviously inferior to TCNTs-1 in the peak current density and onset and peak potentials (Figure S3c). The results indicated that the effect of graphene-like edges on TCNTs was slight compared with the effect of pentagon.

a

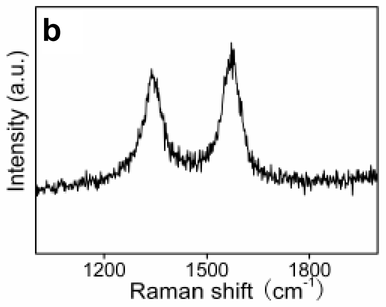

c

Figure S3. The characterization and the activity for ORR of CNTs-D. (a) TEM image, (b) Raman spectrum and (c) CV curves for TCNTs-1, CNTs-1 and CNTs-D at a scan rate of 50 mV s^{-1} in O_2-saturated 0.1 M NaOH electrolyte.

S5 CV tests of ORR on Pt/C in N_2- and O_2-saturated 0.1 M NaOH electrolyte

Figure S4 presents the CVs of Pt/C catalyst measured in N_2- and O_2-saturated 0.1 M NaOH electrolyte. In the case for O_2-saturated electrolytes, distinct peaks appear around -0.17 V. When the O_2-saturated electrolytes are replaced by N_2-saturated ones, this peak disappears. The results indicate that this peak comes from oxygen reduction.

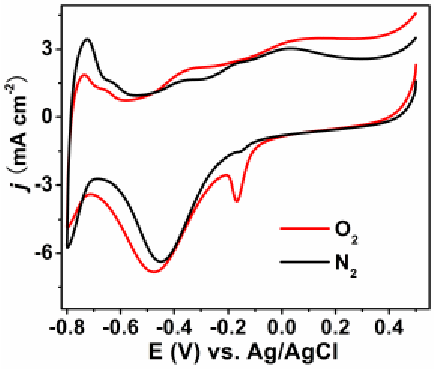

Figure S4. CVs of Pt/C measured in N_2- and O_2-saturated 0.1 M NaOH electrolyte. The scan rate is 50 mV s^{-1}.

S6 The less stable structures for O_2 adsorption on defected PCNT(5,5)/HCNT(5,5).

Apart from the most stable models of the O_2 adsorption on CNT(5,5) and defected PCNT(5,5)/HCNT(5,5) (Figure 6 in the main text), less stable structures for O_2 adsorption on the defected CNT(5,5) at different sites were also shown in Figure S6.

Figure S6. Less stable structures for O_2 adsorptions on pristine and pentagon-/heptagon-doped CNT models (dP/dH: fused pentagon/heptagon; bP: bi-pentagon; PH: fused pentagon-heptagon).

S7 Two relatively stable side-on adsorption structures of O_2 on the CNT(5,5)

The end-on adsorption structure of O_2 on the CNT(5,5) was not stable and here two relatively stable side-on adsorption structures of O_2 on the CNT(5,5) were given (Figure S7). The lower E_{ad} that O_2 side-on adsorption to the CNT(5,5) has to overcome is -1.01 eV (Figure S7b), and hence this model is selected to present as Figure 6 in the main text.

a

b

Figure S7. Side view and top view of two relative stable side-on adsorption structures of O_2 on the CNT(5,5).

S8 Complete reference of Ref. 53 in the main text

Gaussian 09, Revision A.02, Frisch, M. J.; Trucks, G. W.; Schlegel, Scuseria, H. B.; G. E.; Robb, M. A.; Cheeseman, J. R.; Scalmani, G.; Barone, V.; Mennucci, Petersson, B.; G. A.; Nakatsuji, H.; Caricato, M.; Li, X.; Hratchian, H. P.; Izmaylov, A. F.; Bloino, J.; Zheng, G.; Sonnenberg, J. L.; Hada, M.; Ehara, M.; Toyota, K.; Fukuda, R.; Hasegawa, J.; Ishida, M.; Nakajima, T.; Honda, Y.; Kitao, O.; Nakai, H.; Vreven, T.; Montgomery, J. A.; Jr., Peralta, J. E.; Ogliaro, F.; Bearpark, M.; Heyd, J. J.; Brothers, E.; Kudin, K. N.; Staroverov, V. N.; Kobayashi, R.; Normand, J.; Raghavachari, K.; Rendell, A.; Burant, J. C.; Iyengar, S. S.; Tomasi, J.; Cossi, M.; Rega, N.; Millam, J. M.; Klene, M.; Knox, J. E.; Cross, J. B.; Bakken, V.; Adamo, C.; Jaramillo, J.; Gomperts, R.; Stratmann, R. E.; Yazyev, O.; Austin, A. J.; Cammi, R.; Pomelli, C.; Ochterski, J. W.; Martin, R. L.; Morokuma, K.; Zakrzewski, V. G.; Voth, G. A.; Salvador, P.; Dannenberg, J. J.; Dapprich, S.; Daniels, A. D.; Farkas, Ö.; Foresman, J. B.; Ortiz, J. V.; Cioslowski, J.; Fox, D. J. Gaussian, Inc., Wallingford CT, **2009**.